Hindawi
Complexity
Volume 2020, Article ID 3102729, 15 pages
https://doi.org/10.1155/2020/3102729

Research Article

Joint Virtual Energy Storage Modeling with Electric Vehicle Participation in Energy Local Area Smart Grid

Rui-Cheng Dai,[1] Bi Zhao,[1] Xiao-Di Zhang,[1] Jun-Wei Yu,[2] Bo Fan,[3] and Biao Liu[2]

[1]*State Grid Beijing Electric Maintenance Company, Beijing 100080, China*
[2]*State Grid Xinjiang Urumchi Electric Power Supply Company, Urumchi 830011, China*
[3]*Office of Scientific Research and Development Wuhan University, Wuhan 430072, China*

Correspondence should be addressed to Xiao-Di Zhang; 534053362@qq.com

Received 4 July 2020; Revised 17 August 2020; Accepted 12 October 2020; Published 28 October 2020

Academic Editor: Jingang Lai

In this research, the joint virtual energy storage modeling with electric vehicle participation in energy local area Smart Grid is considered. This article first constructs a virtual energy storage model and a joint virtual energy storage model for air conditioning and electric vehicles. Therefore, for the optimization problem of virtual energy storage power, a continuous rolling optimization algorithm to determine the feasible solution of the high-dimensional complex constraint optimization problem is proposed to solve the optimization problem. Finally, the analysis, for example, illustrates the economics of joint virtual energy storage in the Smart Grid. The results prove that air conditioning and electric vehicles have the ability to jointly participate in virtual energy storage, and the comparison proves that joint virtual energy storage can effectively improve the economics of electricity consumption.

1. Introduction

Due to the access of large-scale distributed power equipment, especially the strong randomness of wind power and solar energy, energy storage capacity is of vital importance in the Smart Grid [1–5]. However, batteries are expensive and easily cause pollution [6]. In recent years, a large number of scholars have put forward the concept of virtual energy storage and thus have studied the virtual energy storage with air conditioning participation. The study in [7] analyzes the way of virtual energy storage in the Smart Grid from two aspects: electricity price control and direct control. The study in [8] used the building's heat storage capacity to establish a building-based virtual energy storage system model, by managing the charging (or discharging) power of the virtual energy storage system according to the user's indoor temperature limit and applying it to the microgrid; this literature successfully improved running economy. The study in [9] established a thermodynamic model of air conditioning load with the air conditioning set value as the dependent variable and used it to absorb the strong random distributed new energy power generation equipment output, which improved the energy utilization as well as the stability of the system operation. The study in [10] conducted an in-depth analysis of the direct controllability of some demand-side loads and thus dug into the potential of air conditioning load virtual energy storage. Based on the premise of satisfying the user's comfort requirements, relying on its virtual energy storage to suppress the output of distributed wind turbines with strong randomness, in order to reduce the configuration capacity of energy storage equipment and reduce the cost of energy Internet management regulation, for the controllable load equipment air conditioning, with consideration of its load-adjustable space, the study in [11] established an air conditioning load double-layer optimal scheduling and control model and maximized the interests for both parties through the coordination and optimization between the macrolevel power company and the microlevel direct load control agents. The study in [12–14] improves the economy of energy consumption through the demand response of air conditioning and refrigerator, respectively, on the premise that user comfort can be guaranteed. Although

the virtual energy storage is not explicitly proposed, describing control objects with controllable load and demand response instead, the control method is consistent with that in the research of virtual energy storage.

Furthermore, there are many optimization algorithms applied to multienergy optimization [15, 16] in Smart Grid. In literature [17], a hybrid constraint handling strategy (HCHS) based on nondominated sorting genetic algorithm II (NSGAII) is proposed to deal with the typical constraints, by which the constraint violations can be removed in several steps during the evolutionary process. The study in [1] proposed an artificial shark optimization (ASO) method to remove the limitation of existing algorithms for solving the economical operation problem of microgrid. The study in [18] presents a new metaheuristic optimization algorithm, the firefly algorithm, and an enhanced version of it, called chaos mutation firefly algorithm (CMFA), for solving power economic dispatch problems while considering various power constraints such as valve-point effects, ramp rate limits, prohibited operating zones, and multiple generator fuel options. In literature [19], an improved genetic algorithm is proposed to overcome the obstacle of infeasibility and exhibit better economic dispatch. The study in [20] proposes a new distributed method, namely, the neural-network-based Lagrange multiplier selection (NN-LMS), to prominently reduce the iterations and avoid an oscillation. A calibrated building simulation model was developed in literature [21] and used to assess the effectiveness of demand response strategies under different time-of-use electricity tariffs in conjunction with zone thermal control.

This article first constructs a virtual energy storage model and a joint virtual energy storage model for air conditioning and electric vehicles. Therefore, for the optimization problem of virtual energy storage power, a continuous rolling optimization algorithm to determine the feasible solution of the high-dimensional complex constraint optimization problem is proposed to solve the optimization problem. Finally, the analysis, for example, illustrates the economics of joint virtual energy storage in the Smart Grid.

2. Virtual Energy Storage Modeling with Air Conditioning and Electric Vehicles Participation

2.1. The Overall Structure of Virtual Energy Storage System with Air Conditioning Participation

2.1.1. Physical Model of Virtual Energy Storage with Air Conditioning Participation. For the air conditioning and building virtual energy storage system that relies on temperature for adjustment, the overall structure diagram is shown in Figure 1.

The virtual energy storage of air conditioning and building can be abstracted as a closed-loop system with feedback as shown in Figure 2.

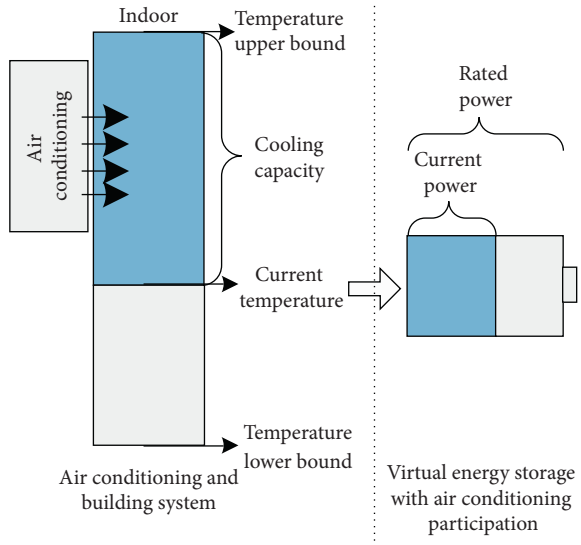

Figure 1: Schematic diagram for virtual energy storage with air conditioning participation.

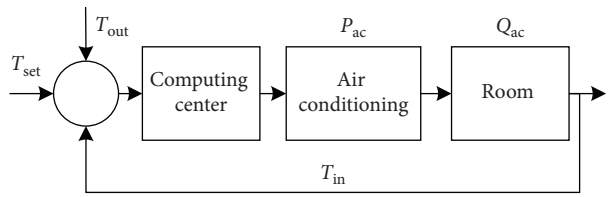

Figure 2: Schematic diagram of a closed-loop system in virtual energy storage with air conditioning participation.

2.1.2. Thermodynamic Model of Thermoelectric Conversion of Air Conditioning. The commonly used thermodynamic equivalent equations [22, 23] are expressed as follows:

$$\frac{dT_{in}(t)}{dt} = \frac{Q_{ac}(t)}{SC} + \frac{(T_{out}(t) - T_{in}(t))}{RSC}. \quad (1)$$

In equation (1), $T_{in}(t)$ and $T_{out}(t)$ are the indoor and outdoor temperatures, respectively, in units of °C; $Q_{ac}(t)$ is the air conditioning cooling capacity, in units of kW; R is the equivalent thermal resistance, in units of °C/kW; C is the building equivalent heat capacity, in units of kJ/°C; S is the building area. The above environmental parameters all have an impact on the virtual energy storage capacity of the air conditioning.

The relationship between the electric power of the air conditioning equipment and the cooling capacity is as follows:

$$P_{ac}(t) = \frac{Q_{ac}(t)}{\eta}. \quad (2)$$

$P_{ac}(t)$ is the air conditioning power in kW; η is the air conditioning thermoelectric conversion coefficient.

2.2. Important Parameters of Virtual Energy Storage with Air Conditioning Participation

2.2.1. Air Conditioning Virtual Energy Storage Remaining Power and Rated Capacity. When the indoor temperature reaches the comfort zone boundary, if the virtual energy storage remaining power is set to 0, it can be determined that, at time t, the air conditioning virtual energy storage power $S_{\text{ac-virtual}}(t)$ is

$$S_{\text{ac-virtual}}(t) = \begin{cases} \dfrac{\text{SC}\left(T_{\max} - T_{\text{in}}(t)\right)}{\eta}, & \text{summer}, \\ \dfrac{\text{SC}\left(T_{\text{in}}(t) - T_{\min}\right)}{\eta}, & \text{winter}. \end{cases} \tag{3}$$

Besides, the expression of air conditioner virtual energy storage rated capacity $S_{\text{ac-virtual-}N}$ is

$$S_{\text{ac-virtual-}N} = \frac{\text{SC}\left|T_{\max} - T_{\min}\right|}{\eta}. \tag{4}$$

From the above derivation, the relationship among the remaining power of virtual energy storage, the rated capacity, and the equivalent heat capacity of the building as well as the comfortable temperature range of the human body can be clearly shown.

2.2.2. Natural Power Consumption in Virtual Energy Storage with Air Conditioning Participation. For the virtual energy storage with air conditioner participation, when the indoor and outdoor temperatures are different, there is always heat exchange in the air conditioning and building virtual energy storage system. At this time, the air conditioning needs a certain amount of power to maintain the indoor temperature equal to the set temperature, that is, natural power consumption for virtual energy storage of air conditioning:

$$P_{\text{ac-}o}(t) = \frac{Q_{\text{s}}(t)}{\eta} = -\frac{T_{\text{out}}(t) - T_{\text{in}}(t)}{\eta R}. \tag{5}$$

$P_{\text{ac-}o}(t)$ will change according to the change of indoor and outdoor temperatures. When the air conditioner power is $P_{\text{ac-}o}(t)$, the balance of indoor and outdoor temperature can be maintained.

2.2.3. Virtual Charge and Discharge Power of Virtual Energy Storage with Air Conditioning Participation. When the air conditioning is running, in the time period which contains time t, it can be known from equation (2) that its average operating power is $P_{\text{ac}}(t)$. Considering the natural loss of electric energy of the air conditioner virtual energy storage $P_{\text{ac-}o}(t)$, the virtual power of the air conditioning virtual energy storage is shown in the following equation:

$$P_{\text{ac-virtual}}(t) = P_{\text{ac}}(t) - P_{\text{ac-}o}(t). \tag{6}$$

In equation (6), $P_{\text{ac-virtual}}(t)$ is the virtual power of the virtual energy storage that the air conditioning participates in. For equation (1), within a period of time, the temperature in the room where the air conditioner works will change to the set temperature, where τ is the length of the time period. Then, equation (1) has

$$\Delta T_{\text{in}}(t) = T_{\text{set}}(t) - T_{\text{in}}(t), \tag{7}$$

$$\Delta t = \tau. \tag{8}$$

After organization,

$$T_{\text{set}}(t) - T_{\text{in}}(t) = \tau \times \left(\frac{Q_{\text{ac}}(t)}{\text{SC}} + \frac{\left(T_{\text{out}}(t) - T_{\text{in}}(t)\right)}{\text{RSC}}\right). \tag{9}$$

After calculation with respect to equation (2), the relationship between the air conditioning power and the indoor and outdoor temperature as well as the set temperature and the length of the time period in the t^{th} time period is obtained as follows:

$$P_{\text{ac}}(t) = \frac{\text{RSC}T_{\text{set}}(t) - (\text{RSC} - \tau)T_{\text{in}}(t) - \tau T_{\text{out}}(t)}{\tau\eta R}. \tag{10}$$

Equations (2), (5)–(7), and (10) are combined to obtain the relationship between the virtual charging power and temperature of the virtual energy storage as follows:

$$P_{\text{ac-virtual}}(t) = \frac{\text{SC}\left(T_{\text{set}}(t) - T_{\text{in}}(t)\right)}{\tau\eta}. \tag{11}$$

2.3. The Overall Structure of the Virtual Energy Storage System with the Participation of Electric Vehicles.

The schematic diagram of virtual energy storage with electric vehicle participation is shown in Figure 3.

The total capacity of the electric vehicle battery is fixed. The battery capacity of each electric vehicle can be used for energy storage in addition to the daily required power. Therefore, the amount of electricity that can be used for virtual energy storage of a single electric vehicle can be determined, and then the total virtual energy storage power of the electric vehicle cluster can be determined.

2.4. Important Parameters of Virtual Energy Storage for Electric Vehicle Participation

2.4.1. Rated Capacity of Virtual Energy Storage for Electric Vehicle Clusters. Let the number of electric vehicles in the i^{th} region at time t be $\text{NE}_i(t)$, the electric vehicles arriving be $\text{NE}_{\text{arrive},i}(t)$, the electric vehicles leaving be $\text{NE}_{\text{leave},i}(t)$, and the number of distributed charging piles be P_i. Then in the period of time t, the maximum controllable number of electric vehicles in the entire area is shown in

$$\begin{aligned} \max \text{NE}_i(t) = {} & \max \text{NE}_i(t-1) + \max \text{NE}_{\text{arrive},i}(t) \\ & - \min \text{NE}_{\text{leave},i}(t). \end{aligned} \tag{12}$$

Then in the area i, the number of electric vehicles participating in the virtual energy storage in the time period t is shown in

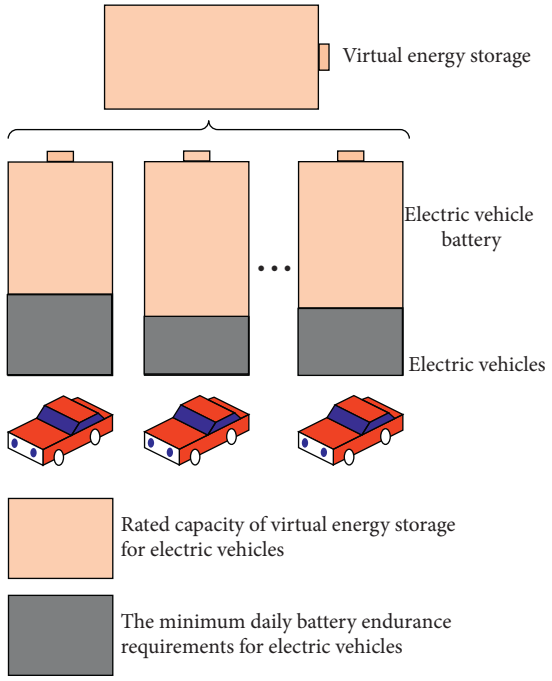

Figure 3: Schematic diagram of the virtual energy storage process of electric vehicles.

$$\mathrm{NE}_i(t) = \min\left(P_i, \max \mathrm{NE}_i(t)\right). \tag{13}$$

Then for the remaining energy in the virtual energy storage at different times in the area i, equation (14) is as follows:

$$S_{\mathrm{EV-virtual},i}(t) = \sum_{j=1}^{\mathrm{NE}_i(t)} \left(W_{j,i}(t) - W_{j,i}^0\right). \tag{14}$$

In equation (14), $S_{\mathrm{EV-virtual},i}(t)$ is the virtual energy storage capacity of electric vehicles in the period of t in the i^{th} region; $W_{j,i}(t)$ is the remaining power of the j^{th} electric vehicle in the i^{th} region in the time period t; $W_{j,i}^0$ is the minimum electric power required for the j^{th} electric car in the i^{th} area, which does not change with time.

Then, the rated energy storage of electric vehicles in the i^{th} area is

$$S_{\mathrm{EV-virtual},i,N}(t) = \sum_{j=1}^{\mathrm{NE}_i(t)} \left(W_{j,i,N}(t) - W_{j,i}^0\right), \tag{15}$$

where $S_{\mathrm{EV-virtual},i,N}(t)$ is the rated energy storage capacity of the virtual energy storage in the time period t and $W_{j,i,N}(t)$ is the rated battery capacity of the j^{th} electric vehicle in the area i in the time period t.

2.4.2. Virtual Charging and Discharging Power for Virtual Energy Storage of Electric Vehicles. The charge and discharge power of the virtual energy storage of electric vehicles can be expressed by the following equation:

$$P_{\mathrm{EV-virtual},i}(t) = P_{\mathrm{EV}} \times \mathrm{NE}_i(t). \tag{16}$$

In equation (16), P_{EV} is the charging and discharging power of the electric vehicle charging and discharging piles, $P_{\mathrm{EV-virtual},i}(t)$ is the virtual charging power of the virtual energy storage of the electric vehicle in the area i with time period which includes time t, and $\mathrm{NE}_i(t)$ is the number of electric vehicles participating in the virtual energy storage in the area i with time period which includes time t.

From the perspective of the electric vehicle's virtual energy storage capacity, its charging power meets

$$P_{\mathrm{EV-virtual},i,\mathrm{in}}(t) = \frac{S_{\mathrm{EV-virtual},i,N}(t) - S_{\mathrm{EV-virtual},i}(t)}{\tau}. \tag{17}$$

From the perspective of the virtual energy storage capacity of electric vehicles, the discharge power meets

$$P_{\mathrm{EV-virtual},i,\mathrm{out}}(t)\frac{S_{\mathrm{EV}v,i}}{\tau}. \tag{18}$$

In equations (17) and (18), τ is the length of the discharge time period.

3. Construction of the Mathematical Model of Joint Virtual Energy Storage Optimization Based on the Rolling Optimization Method

Aiming at the problem of determination of high-dimensional complex constraint decision variables in global optimization of electric vehicle virtual energy storage model, this paper proposes a feasible solution continuous rolling correction algorithm.

Aiming at the global optimization problem of electric vehicle virtual energy storage output power, during the initialization process, due to the complexity of mutual coupling of local constraints and global constraints, the probability of obtaining a feasible solution is low, and initialization cannot be completed. In order to solve the above problems, this paper proposes constructing a standard function to measure the global constraint error that satisfies the local constraint decision variables during initialization and thus continuously revising the decision variables through continuous rolling optimization. Experiments show that this method can effectively improve the initialization efficiency of complex constrained optimization problems with high-dimensional decision variables and then obtain the global optimized output power of electric vehicle virtual energy storage, which verifies the economics of electric vehicle with the combination of virtual energy storage.

3.1. Rolling Optimization Process. For the value of the virtual energy storage power in different time periods, the optimization result of the previous period will affect the virtual energy storage power range in the next period. Drawing on the idea of rolling optimization, the value of virtual energy storage power can be adjusted continuously with the advancement of the sampling time to determine the power of virtual energy storage in each period. The process is shown in Figure 4.

The state in the time period t mainly includes the outdoor temperature and the number of arriving and leaving

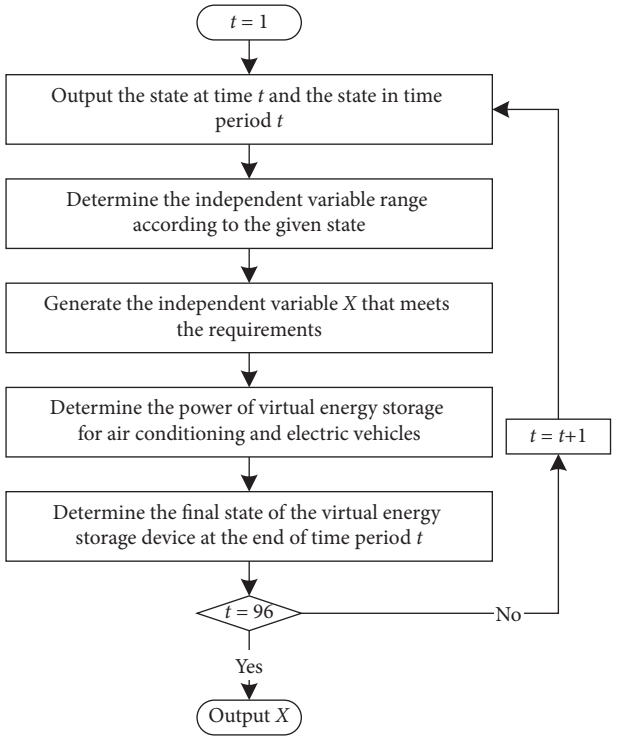

Figure 4: Flowchart of virtual energy storage capacity and output power rolling optimization.

electric vehicles as well as the remaining power of the power battery. The state at time t refers to the indoor temperature at time t and the total remaining capacity of the electric vehicle's virtual energy storage at time t.

For the virtual energy storage in which air conditioning participate,

$$T_{\text{in}}(t+1) = T_{\text{set}}(t) = \frac{\text{SCT}_{\text{in}}(t) + \tau\eta P_{\text{acv}}(t)}{\text{SC}}. \tag{19}$$

For electric vehicles, for the virtual energy storage state at time $t+1$ during the rolling optimization process in the region i, when the virtual energy storage state $S_{\text{EV-virtual},i}(t)$, the input power $P_{\text{EV-virtual-}in}(t)$, and the output power $P_{\text{EV-virtual-out}}(t)$ at the previous time are known, the status of the virtual energy storage capacity of electric vehicles at the beginning of the next time period can be determined:

$$\begin{aligned} S_{\text{EV-virtual},i}(t+1) = {} & S_{\text{EV-virtual},i}(t) - P_{\text{EV-virtual-out}}(t) \\ & \times \tau + P_{\text{EV-virtual-in}}(t) \times \tau. \end{aligned} \tag{20}$$

3.2. Objective Function. In the case where other conditions are certain and uncontrollable, for the virtual energy storage optimization scheduling in which air conditioning and electric vehicles jointly participate, the optimization objective function has the lowest total cost of electricity consumption throughout the day:

$$\begin{aligned} \min C = \min & \sum_{t=1}^{T}\sum_{i=1}^{M}\left(C_{\text{WT},i}(t) + C_{\text{PV},i}(t) + C_{\text{grid},i}(t)\right) \\ & + \sum_{i=1}^{M}\left(C_{\text{EV},i} + C_{\text{AC},i}\right). \end{aligned} \tag{21}$$

In equation (21), M is the total number of residential area and units in the area; in the area i at the time t, $C_{\text{WT},i}(t)$ and $C_{\text{PV},i}(t)$ are the total cost of wind power and photovoltaic power, respectively; $C_{\text{grid},i}(t)$ is the cost of purchasing electricity from the power grid; $C_{\text{EV},i}$ is the cost of virtual energy storage with electric vehicles participation in the area i throughout the day; $C_{\text{AC},i}$ is the cost of air conditioning virtual energy storage throughout the day in the area i.

In addition,

$$\begin{aligned} C_{\text{WT},i}(t) &= p_{\text{WT},i,\text{repare}} \times E_{\text{WT},i}(t), \\ C_{\text{PV},i}(t) &= p_{\text{PV},i,\text{repare}} \times E_{\text{PV},i}(t). \end{aligned} \tag{22}$$

In equation (22), $p_{\text{WT},i,\text{repare}}$ and $p_{\text{PV},i,\text{repare}}$ are the power generation maintenance costs of wind turbines and photovoltaic power generation, respectively. And their units are CNY/kWh; $E_{\text{WT},i}(t)$ and $E_{\text{PV},i}(t)$ are the power generation capacity of wind turbines and photovoltaic power generation during the time period which contains time t:

$$C_{\text{grid},i}(t) = p_{\text{grid}}(t) \times E_{\text{grid},i}(t). \tag{23}$$

In equation (23), $p_{\text{grid}}(t)$ is the price of electric energy in the time period which contains time t, which can be step price, peak-valley price, time-sharing price, or real-time price, and $E_{\text{grid},i}(t)$ represents time t:

$$C_{\text{EV},i} = p_{\text{EV}} \times E_{\text{EV},i}. \tag{24}$$

In equation (24), p_{EV} is the cost of virtual energy storage with electric vehicles participation; the unit is CNY/kWh; $E_{\text{EV},i}$ is the total amount of virtual energy storage with electric vehicles participation in the i^{th} area in the whole day:

$$C_{\text{AC},i} = p_{\text{AC}} \times E_{\text{AC},i}. \tag{25}$$

In equation (25), p_{AC} is the cost of in virtual energy storage with air conditioning participation; the unit is CNY/kWh; $E_{\text{AC},i}$ is the total amount of virtual energy storage with air conditioning participation in the i^{th} area throughout the day.

3.3. Restrictions

3.3.1. Energy Balance Constraint. The output power of all power sources and energy storage devices at time t should be

equal to the electricity consumption at that time, as shown in equation (26):

$$P_{\text{ac}-o} + P_{\text{EV}-o} + \text{demand} = P_{\text{WT}} + P_{\text{PV}} + P_{\text{ac-virtual}} + P_{\text{grid}} + P_{\text{EV-virtual}}. \quad (26)$$

$P_{\text{ac}-o}$ is the natural power consumption load curve of the virtual energy storage of the air conditioning, $P_{\text{EV}-o}$ is the charging power load curve of the electric vehicle, demand is the daily load demand, P_{WT} is the wind power, P_{PV} is the photovoltaic power, $P_{\text{ac-virtual}}$ is the input (or output) power of the virtual energy storage with air conditioning participation, P_{grid} is the power of the power grid, and $P_{\text{EV-virtual}}$ is the input (or output) power of the virtual energy storage involved in electric vehicles.

3.3.2. Output Power Constraints. Any distributed power supply and virtual energy storage device have a limitation for power rating, as shown in equation (27):

$$P_{i,\min}(t) < P_i(t) < P_{i,\max}(t). \quad (27)$$

In this equation, $P_{i,\min}(t)$ and $P_{i,\max}(t)$ are the minimum and maximum values of the average output power of the i^{th} device in the period of time t, respectively.

3.3.3. Restrictions on the Basic Driving Power Demand of the Next Day after the Electric Vehicle Participates in the Virtual Energy Storage. The remaining power of any electric vehicle can at least meet the needs of traveling the next day, as shown in equation (28):

$$W_{j,i} - W^0_{j,i} > 0. \quad (28)$$

$W_{j,i}$ is the remaining power of the j^{th} electric car in the i^{th} area, and $W^0_{j,i}$ is the minimum power required for the j^{th} electric vehicle in the i^{th} area.

The remaining power constraint for electric vehicles is participating in virtual energy storage.

The remaining power of virtual energy storage cannot be negative:

$$S_{\text{EV-virtual},i} > 0. \quad (29)$$

$S_{\text{EV-virtual},i}$ is the remaining power of the i^{th} electric vehicle.

4. Continuous Rolling Optimization of Feasible Solution Initialization for High-Dimensional Complex Constrained Optimization Problem

By analyzing the rolling optimization model proposed above, we can find that the model built in this chapter has the following characteristics:

(1) The dimension of decision variables is high

(2) There are local constraints described by the rolling optimization model among decision variables

(3) There are global constraints on decision variables

This section proposes a continuous rolling optimization algorithm for initializing feasible solutions for high-dimensional complex constrained optimization problems for rolling optimization models and complex constraints, so as to obtain decision variables that simultaneously satisfy multiple types of constraints.

4.1. Treatment Strategy for Multiconstraint Problems. A large number of inequality constraints will result in multiple feasible regions with irregular shapes in the feasible solution space, and the decision variables must satisfy all the constraints, which requires the determination of the range of feasible regions. Take the feasible region of a two-dimensional optimization problem as an example, as shown in Figure 5.

In the figure shown above, A_1 and A_2 are, respectively, feasible regions of decision variables for two different constraints. Since the area of A_2 is small, processing the constraints in parallel will greatly reduce the probability of the decision variable falling in A_2. This will make it difficult for a large number of decision variables to meet the A_2 constraint conditions, resulting in inefficient decision variable selection. However, when the problem to be solved is a high-dimensional optimization problem, the shape of the feasible region corresponding to the constraint conditions is more difficult to determine, and the intersection between the feasible regions is also more difficult to obtain. For the optimization problems shown in this chapter, the dimension of its solution space is shown in equation (30) as follows:

$$D = D_1 + D_2 = N_1 \times T_1 + N_2 \times T_2. \quad (30)$$

In equation (30), N_1 and N_2 are the number of time periods divided per hour, which are both 4 in the questions in this chapter. Besides, T_1 and T_2 are the total time of the optimization cycle, which are both 24 in this paper, so for the optimization problem given in this chapter, its dimension is 192. In practical problems, as the influence factors considered increase, its dimensions may become larger.

4.2. Solution Feasible Probability. For the determination of the feasible solution with multiple constraints, this section uses the solution feasible probability to evaluate its efficiency, as shown in equation (31):

$$P_{(A_1 \cap A_2)/(A_1)} = \frac{P_{A_1 \cap A_2}}{P_{A_1}}. \quad (31)$$

The following is an analysis of its value, first of all for the one-dimensional optimization problem. The feasible solution selection process is shown in Figure 6.

In the two one-dimensional constraints given in the above figure, if N feasible solutions are determined in parallel, the process is to first generate N feasible solutions for A_1 constraint in the $[x_1, x_2]$ interval and then judge whether it meets A_2. According to the range covered by A_1 and A_2, we can know the solution feasible probability when the feasible solutions are evenly distributed:

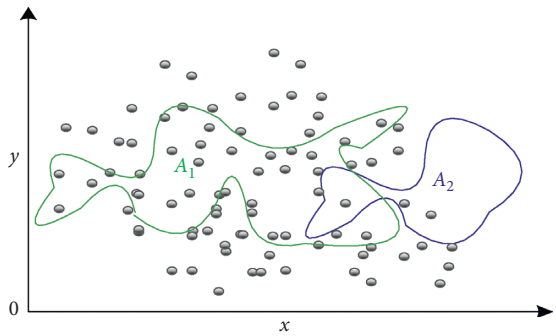

Figure 5: Schematic diagram of the feasible domain for the solution of a two-dimensional optimization problem.

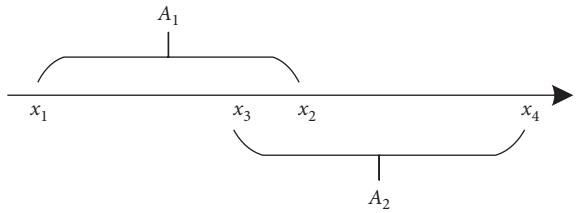

Figure 6: Schematic diagram of feasible solutions for one-dimensional optimization problems.

$$P_{(A_1 \cap A_2)/(A_1)} = \frac{P_{A_1 \cap A_2}}{P_{A_1}} = \frac{x_2 - x_3}{x_2 - x_1}. \tag{32}$$

Claim: after choosing a feasible solution with A_1 constraint, the probability of satisfying A_2 constraint is $P_{(A_1 \cap A_2)/(A_1)}$.

The following dimension of the optimization problem is increased. In the two-dimensional optimization problem, the solution feasible probability is discussed. The simpler inequality constraint is selected; thus, the selection process of a feasible solution is shown in Figure 7.

The feasible probability is shown in

$$P_{(A_1 \cap A_2)/(A_1)} = \frac{P_{A_1 \cap A_2}}{P_{A_1}} = \frac{x_2 - x_3}{x_2 - x_1} \times \frac{y_2 - y_3}{y_2 - y_1}. \tag{33}$$

According to the solution feasible probability of the low-dimensional complex constrained optimization problem, if its $P_{(A_1 \cap A_2)/(A_1)}$ in each dimension is P, then the solution feasible probability of the N-dimensional multiconstrained optimization problem should be P^N. When N is too large, the probability of its feasible solution selection probability will be very small, and it is easy to make the optimization process fall into an infinite loop. The following experiment determines the feasible probability of the solution of the optimization problem in different dimensions and sets P to 0.5. The results are shown in Table 1.

In view of the dimensional disaster in this paper, the undeterminable problem of feasible solutions in this chapter could be analyzed and solved. Therefore, this section proposes a continuous rolling optimization algorithm to solve the inefficiency problem of multiconstrained feasible solutions.

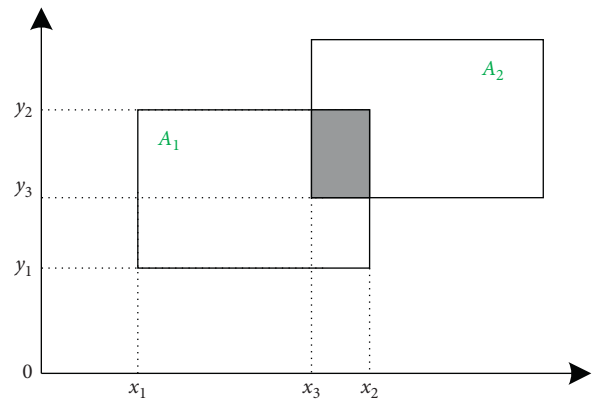

Figure 7: Schematic diagram of the feasible solution of the two-dimensional optimization problem.

Table 1: Probability comparison of random initialization solutions for optimization problems in different dimensions.

The dimension of optimization problem	Solution feasible probability with theoretical calculation (%)	The solution feasible probability error with experimental results (%)
1	50	50
2	25	25
3	12.5	12.5
5	3.125	3.125
10	0.09765625	0.09765625

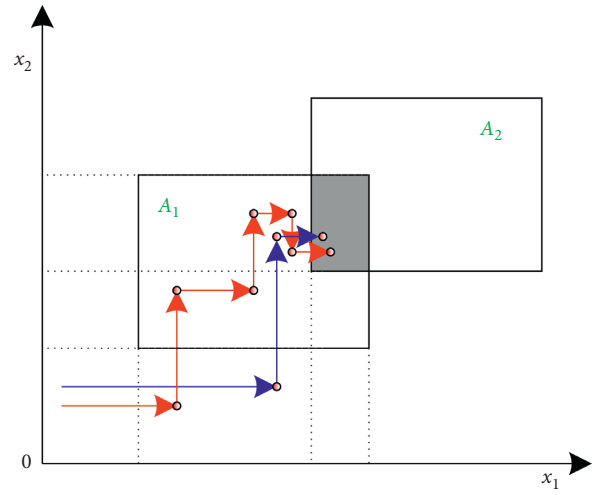

Figure 8: Continuous rolling revision selection process of feasible solutions for two-dimensional optimization problems.

4.3. Algorithm Flow. For the high-dimensional complex constrained optimization problem, the analysis is first based on the two-dimensional optimization problem. When the optimization problem is faced with global constraints and local constraints, the optimization process is shown in Figure 8, where A_1 represents the constraint condition 1 and A_2 represents the constraint condition 2.

In the figure shown above, the red and blue paths are the optimization paths of the results with two consecutive

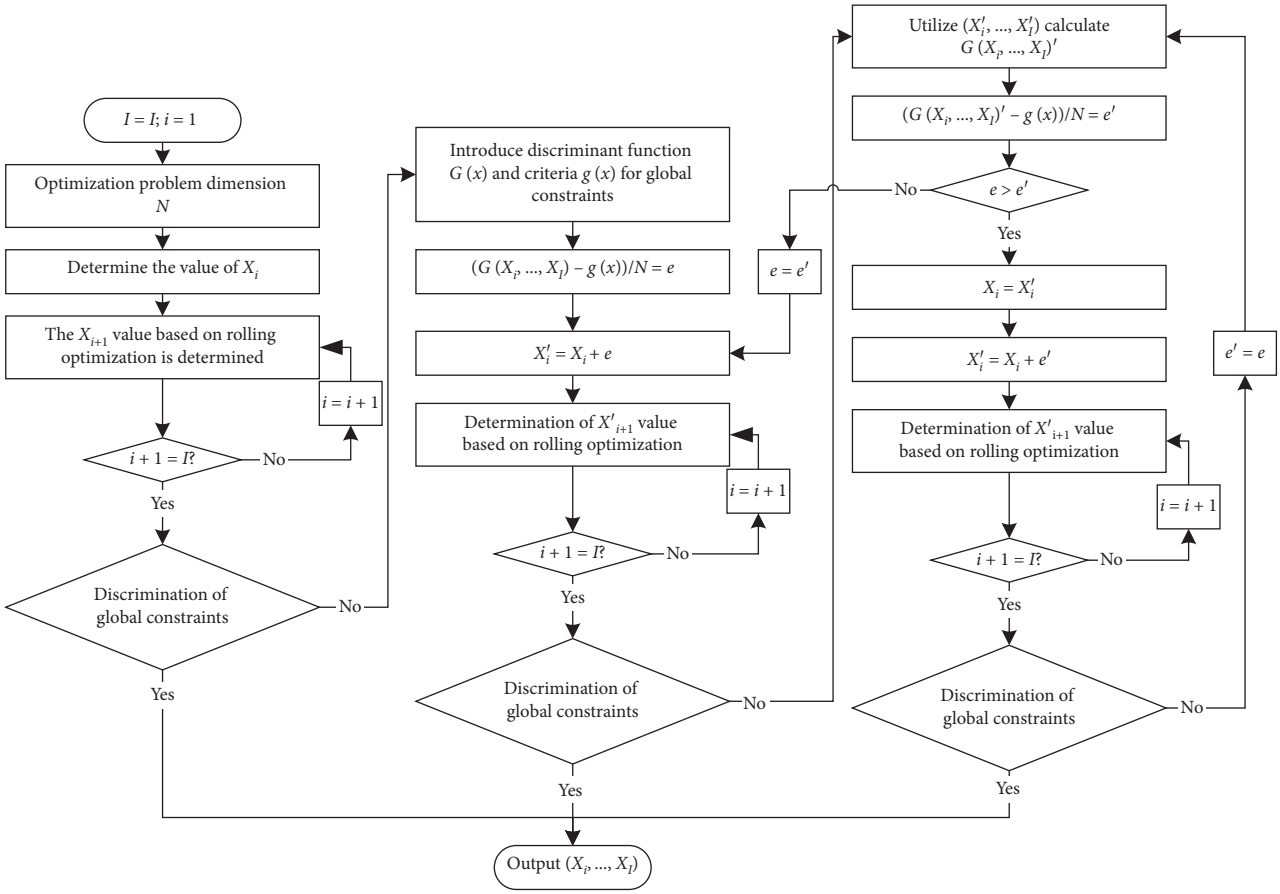

Figure 9: Flowchart of continuous rolling optimization algorithm.

optimizations. Since A_1 represents local constraints and x_1 has a mutual influence with x_2, combined with the rolling optimization model proposed in the previous section, the evolutionary process of the continuous rolling optimization algorithm determined by the local constraint and the global constraint common feasible region of the optimization problem can be determined as shown in Figure 9.

The specific steps are as follows:

(1) Determine the value of the N-dimensional decision variable $x_1, \ldots, x_i$.

(2) Determine whether the global optimization requirements are met; thus, directly output the N feasible domain decision variable $x_1, \ldots, x_i$ if the requirements are all met. Based on the feasible probability of the solution, the N-dimensional decision variable $x_1, \ldots, x_i$ at this time is difficult to meet the requirements; if not, go to step (3).

(3) Introduce the global constraint condition discriminant function $G(x)$, which is related to the constraint condition of the optimization problem, but not directly a constraint condition. It needs to be formulated according to different global constraints. The conditional discriminant function $G(x)$ selected in this chapter is the remaining power of virtual energy storage with electric vehicle participation. Under actual operating conditions, when all electric vehicles leave the residential area, the remaining power of virtual energy storage with electric vehicle participation should be 0, so its standard function $g(x) = 0$.

(4) Determine the average error according to the conditional discriminant function $G(x)$ and its standard function value $g(x)$.

(5) Obtain a new N-dimensional decision variable $x'_1, \ldots, x'_i$ based on $x'_i = x_i + e$, judge whether it meets the global optimization requirements, and directly output the N-dimensional feasible region decision variable $x'_1, \ldots, x'_i$ if it meets all requirements; if not, go to step (6).

(6) Determine the new average error e' based on the N-dimensional feasible region decision variable $x'_1, \ldots, x'_i$ and the global constraint discriminant function $G(x)$, as well as its standard function value $g(x)$.

(7) Compare e with e'; if the error becomes larger after the correlation for average error e (i.e., $e' > e$), then let $e = e'$ and go back to step (5). Recalculate the N-dimensional feasible domain decision variable $x'_1, \ldots, x'_i$; if the error is significantly reduced (i.e., $e' < e$), then update the N-dimensional feasible region decision variable $x_1, \ldots, x_i$, obtain the new N-dimensional decision variable $x'_1, \ldots, x'_i$ for the new

average error e', and then determine whether the global optimization requirements are met; thus, directly output the N-dimensional feasible domain decision variable $x_1', \ldots, x_i'$ if it meets all requirements; if not, go to step (8).

(8) Update the newly generated e' so that $e = e'$; therefore, determine the new average error e' based on the updated N-dimensional feasible domain decision variable $x_1', \ldots, x_i'$, and then go to step (7).

4.4. Optimization Effect Analysis. In the problem solved in this chapter, one of the decision variables is the input and output power of the virtual energy storage with electric vehicle participation in each time period, and the remaining power of the electric vehicle virtual energy storage is used as the standard to detect whether the global optimization is completed. The distribution diagram of the arrival and departure time of electric vehicles in this simulation is shown in Figure 10. The results of the comparison between the unoptimized and optimized global constraint detection standard function values are shown in Figure 11.

As can be seen from Figure 10, the last two vehicles in the area left within the time period of 10:00–10:15 and the total power 47.78 kWh can be determined by calculation.

As can be seen from Figure 11, at 10:00 before rolling optimization, when the last two electric vehicles have not left, the remaining power of virtual energy storage is 154.4 kWh. According to simulation calculations, the remaining power of the two electric vehicles is 47.78 kWh. That is, after the last two vehicles have left, the remaining energy of the virtual energy storage is still not 0, which obviously does not meet the global constraints, indicating that the decision variables fall outside the feasible domain of the global constraints, and the initialization fails. If the continuous rolling optimization algorithm is not adopted, the decision variables need to be initialized again.

After the continuous rolling optimization determined for the high-dimensional complex constraint optimization feasible solution, the results are consistent with the electric vehicle arrival and departure states, indicating that the continuous rolling optimization algorithm [5, 24] for the high-dimensional optimization of global constraints and local constraints that jointly govern the feasible domain can effectively limit the decision variables within the global constraints and local constraints that jointly govern the feasible domain for the problems in this chapter, which helps improve the optimization efficiency.

5. Analysis

This section first simulates the virtual energy storage capacity of air conditioning and electric vehicles and illustrates the feasibility of virtual energy storage. Then virtual energy storage is optimized for scheduling. In the example calculation process, the virtual energy storage power range of air conditioning and electric vehicles is first determined, and then the day is divided into 96 time periods to optimize the virtual energy storage power within the power range.

5.1. Analysis of Air Conditioning and Electric Vehicle Virtual Energy Storage Capacity

5.1.1. Output Power of the Virtual Energy Storage Model with EV Participation. In the virtual energy storage in which electric vehicles participate, the input and output power of the virtual energy storage and the arrival and departure of the electric vehicle will affect the remaining power of the virtual energy storage. Under rolling optimization, the relationship can be obtained by Figure 12.

As can be seen from Figure 12, the continuous energy optimization of the electric vehicle's virtual energy storage output meets the local constraints; the virtual energy storage remaining power becomes 0 after all the electric vehicles leave, indicating that the virtual energy storage output power meets the global constraint conditions.

5.1.2. Output Power of Virtual Energy Storage Model with Air Conditioning Participation. In the virtual energy storage with air conditioning participation, the input and output power of the virtual energy storage and the natural power loss of the virtual energy storage based on the indoor and outdoor temperature difference will affect the remaining power of the virtual energy storage and the change of room temperature. Under rolling optimization, the changes of the above four parameters are shown in Figures 13 and 14.

It can be seen from the comparison that, within the temperature constraint range, the virtual energy storage of the air conditioner can realize the virtual power change of the virtual energy storage through the change of the air conditioner power.

5.2. Determination of the Range of Virtual Energy Storage Power for Air Conditioning and Electric Vehicles

5.2.1. Virtual Energy Storage Charge and Discharge Power Range with EV Participation. For the virtual energy storage of electric vehicles, according to the spatial and temporal distribution of electric vehicles given in Figure 12 and the power demand for driving on the day according to equations (17) and (18), the input and output power range of virtual energy storage with electric vehicles participation can be determined. The results are shown in Figure 15.

5.2.2. Determination of the Range of Charge and Discharge Power at the Starting Time in the Virtual Energy Storage with Air Conditioning Participation. The daily temperature change curve in this area is shown in the red line in Figure 13. Considering the natural consumption rate of the virtual energy storage of the air conditioning, the output power of the virtual energy storage reaches the maximum when the air conditioner is not running, which is $P_{ac-O}(t)$; when the air conditioner is running, its input and output power are shown in equation (11). The maximum value of the virtual energy storage discharge power changes according to the change of the set temperature. The temperatures are set to 19.5°C, 20.5°C, and 21.5°C, respectively;

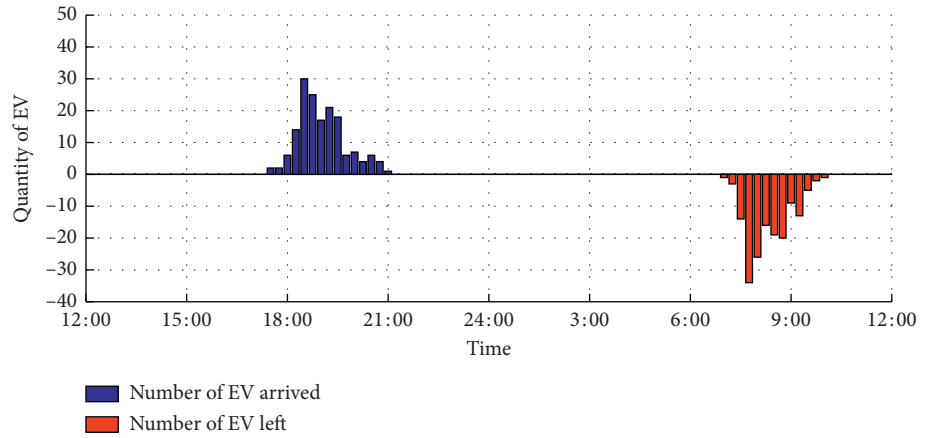

Figure 10: The distribution of vehicle arrival and departure times in this optimization.

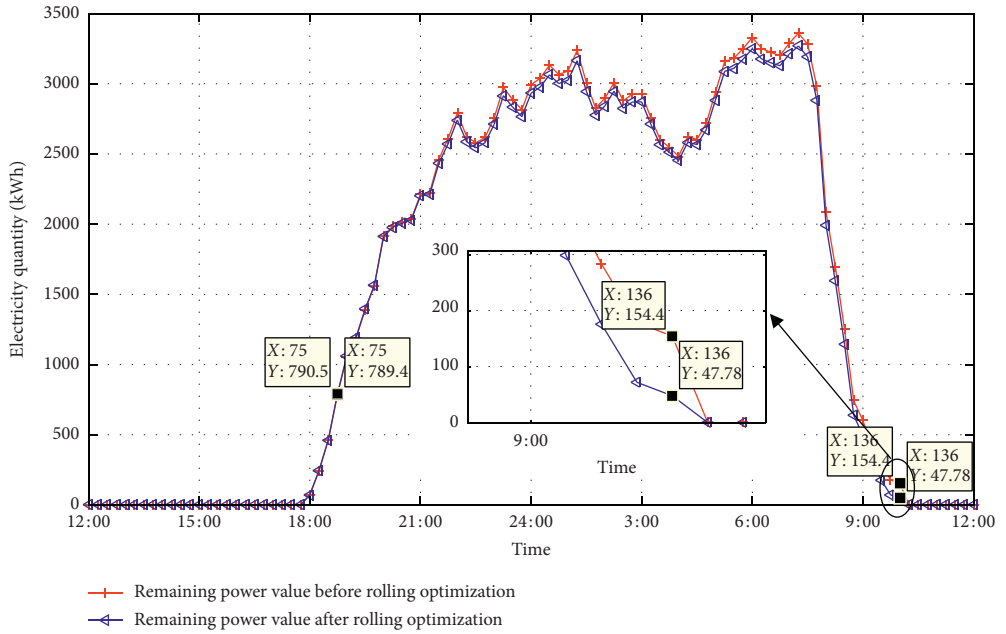

Figure 11: Comparison result of standard function value of global constraint detection.

in the following figure, the upper limit of the virtual energy storage output power changes as shown in Figure 16.

It can be seen from the above figure that the output power of the virtual energy storage decreases as temperature increases.

5.2.3. Economic Analysis of Optimization for Joint Virtual Energy Storage. Based on air conditioning, electric vehicles have the ability to adjust the operating power within a certain range to convert electrical energy into thermal energy storage or perform bidirectional energy exchange with the power grid to achieve the virtual energy storage capacity of energy transfer. The following is the simulation of the effect of virtual energy storage of air conditioning and electric vehicles in this example. Regarding the load of the resident users in the constant temperature community, consider a total of about 650 small high-rise (five-story) households with a total construction area of 65,000 square meters, a total air conditioning power of 1000 kW, and an average of about 1.5 kW per household; on the top floor, there is about 6500 square meters of photovoltaic panels installed, and 10 wind turbines equipped; the power of its distributed power generation equipment is shown in Figure 17.

Considering that virtual energy storage with electric vehicles participation only charges 0.4883 CNY/kWh, so when actually using electric vehicles for virtual energy storage, the discharge cost of electric vehicles is 0.6883 CNY/kWh, and the discharge efficiency is 80%. In addition, the maintenance cost for wind turbines and photovoltaic power generation is shown in Table 2 [8].

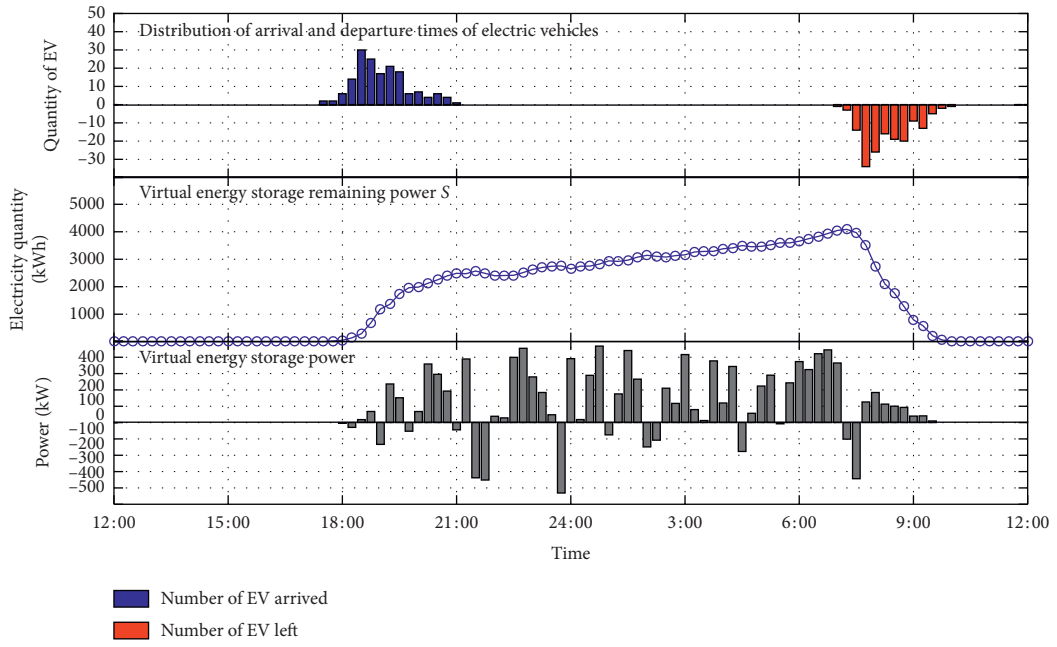

Figure 12: Comparison chart of electric vehicle's space-time distribution, remaining power, and power.

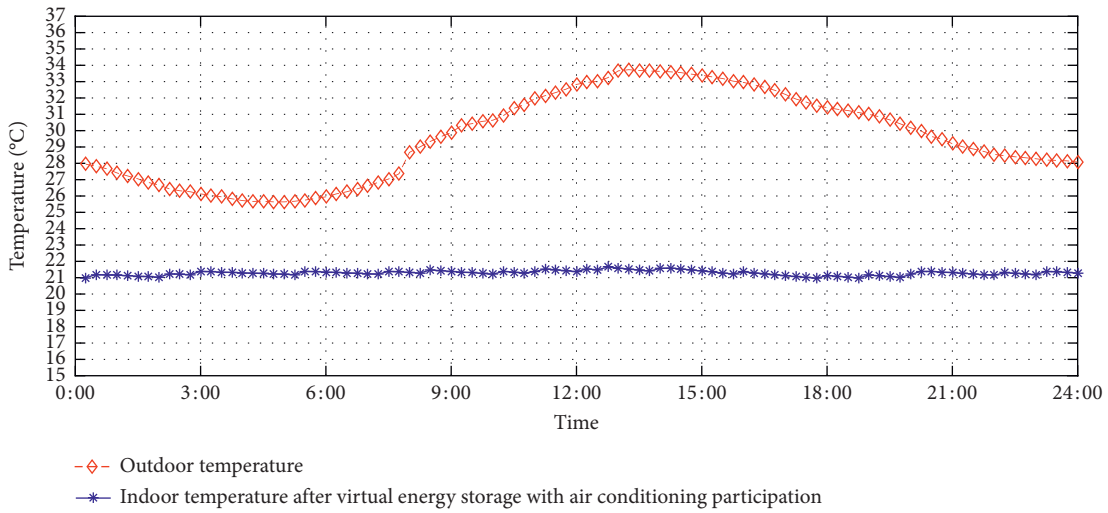

Figure 13: Comparison of indoor and outdoor temperature change curves.

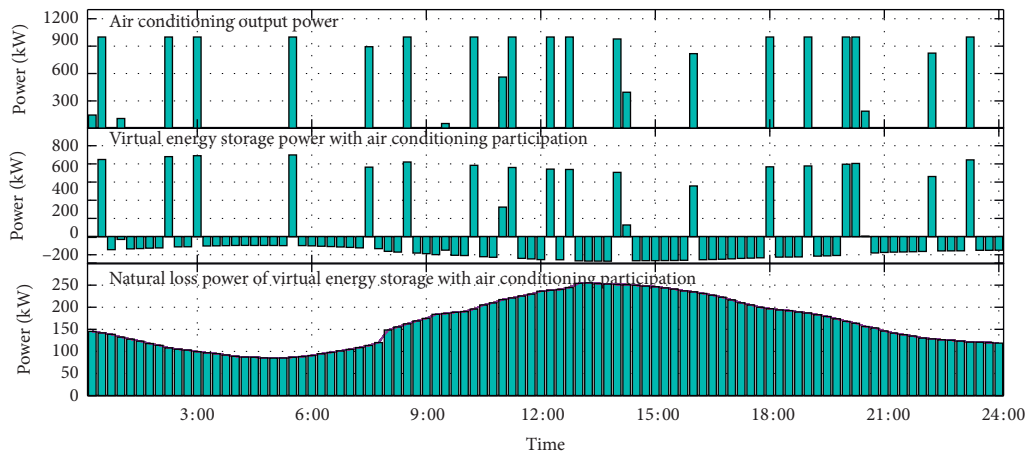

Figure 14: Comparison chart of the natural power consumption of the virtual energy storage with air conditioning participation, air conditioning power, and virtual power of virtual energy storage.

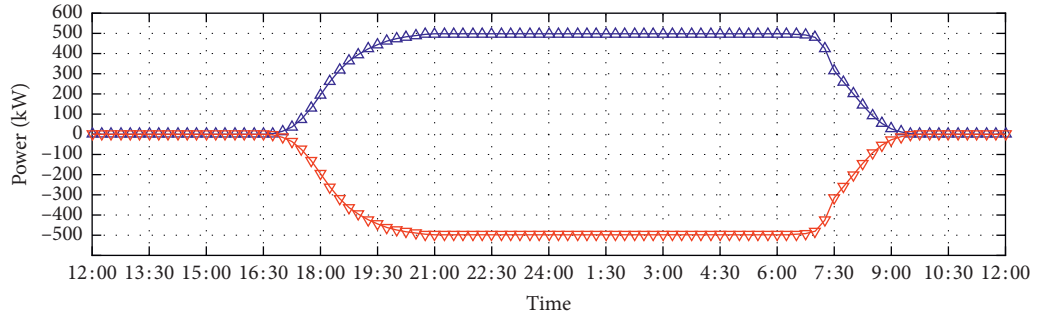

Figure 15: Chart of power range of virtual energy storage with electric vehicle participation.

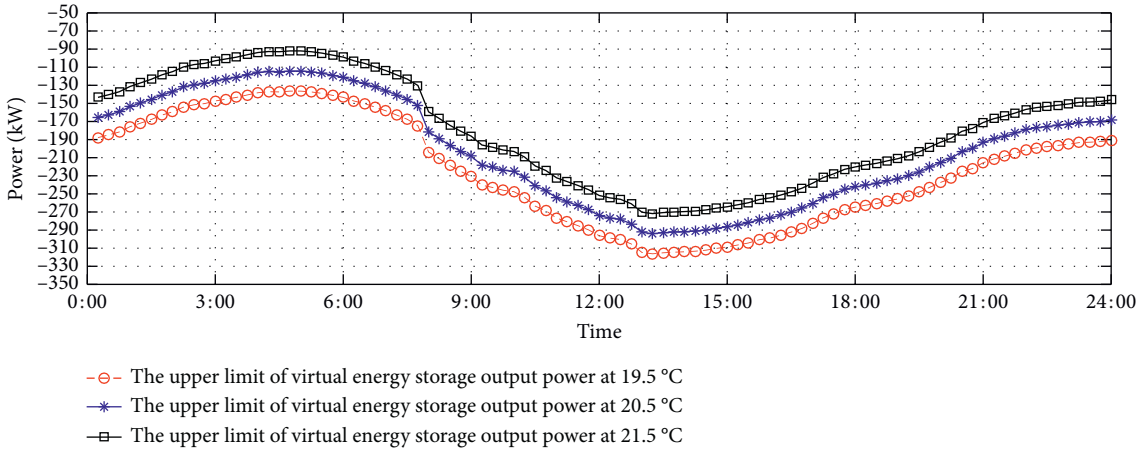

Figure 16: Comparison of the maximum output power of virtual energy storage at different set temperatures.

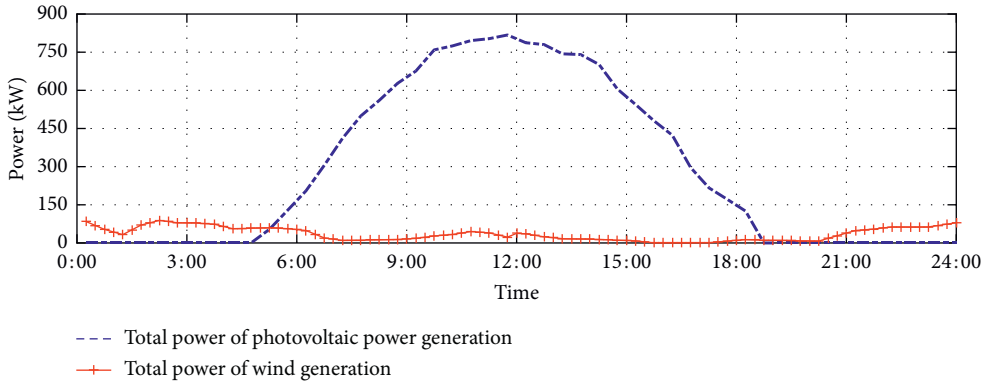

Figure 17: The total power of the wind turbine and photovoltaic power generation of the constant temperature small high-rise building in number 1 residential area.

Table 2: Maintenance cost table for wind turbine and photovoltaic power generation.

Parameter (CNY/kWh)	Value
Wind turbine maintenance cost	0.11
PV maintenance cost	0.08

The total load demand curve of the residents is shown in Figure 18.

This environment corresponds to four scenes, respectively.

Scenario 1. Electric vehicle and air conditioner jointly participate in virtual energy storage.

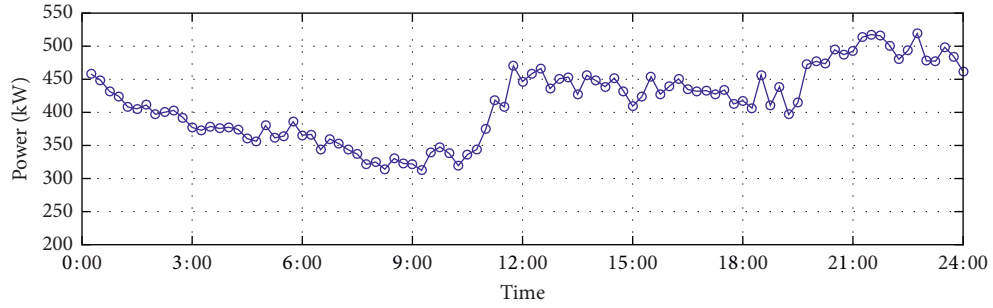

Figure 18: Daily load curve in residential area number 1.

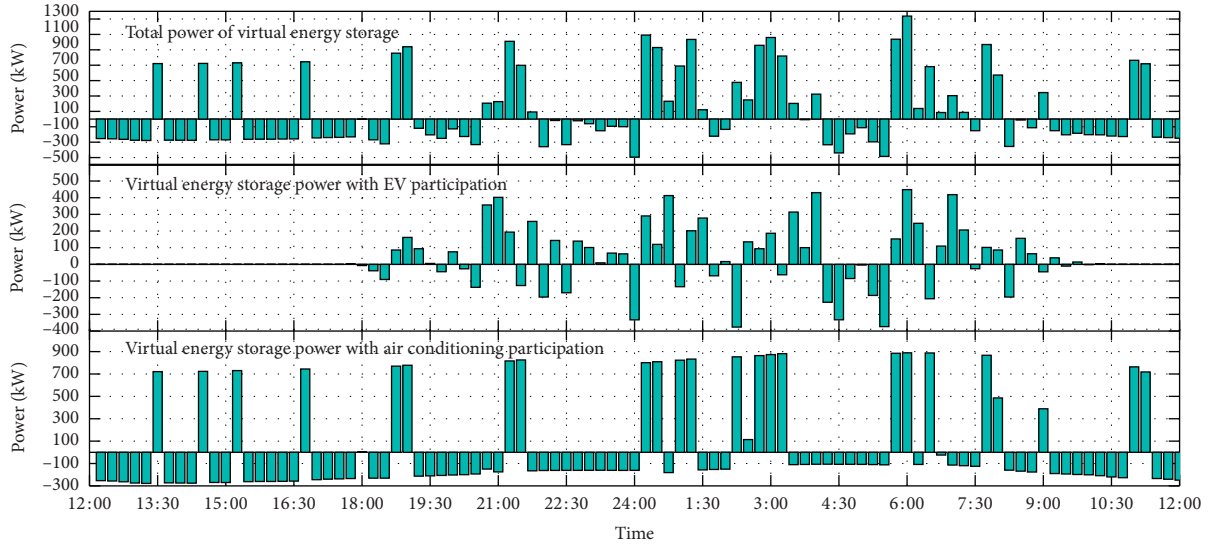

Figure 19: Optimized power of combined virtual energy storage in Scenario1.

Scenario 2. Electric vehicle participates in virtual energy storage.

Scenario 3. Air conditioner participates in virtual energy storage.

Scenario 4. Virtual energy storage is not called.

The economics of these four scenarios are compared as follows.

In Scenario1, the results obtained by air conditioning and electric vehicles participating in virtual energy storage optimization scheduling and the results of using electric vehicles or air conditioning alone to participate in virtual energy storage are shown in Figure 19.

In Scenario2, the results obtained by air conditioners independently participating in virtual energy storage optimization scheduling are shown in Figure 20.

In Scenario3, the results of electric vehicles independently participating in virtual energy storage optimization scheduling are shown in Figure 21.

In the above four scenarios, the comparison results of the total daily electricity charges in the residential area are shown in Table 3.

From the above comparative analysis, the following conclusions can be drawn:

(1) When the joint virtual energy storage of air conditioners and electric vehicles is adopted, the total cost of electricity charges in residential areas can be reduced by 10%.

(2) The photovoltaic power generation in residential areas is highly compatible with the operating time of air conditioners. Therefore, when participating in virtual energy storage alone, the effect of air conditioning participating in virtual energy storage is better than electric vehicles participating in virtual energy storage.

(3) Analyze the reasons for the different total electricity costs in residential areas under different scenarios on a certain day, mainly because air conditioning and electric vehicles can store the electrical energy generated by new energy power generation equipment, which reduces the phenomenon of wind and heat rejection, realizes the efficient utilization of new energy power generation equipment, and also reduces the cost of purchasing electricity from the power grid. Therefore, it has also proved that the joint

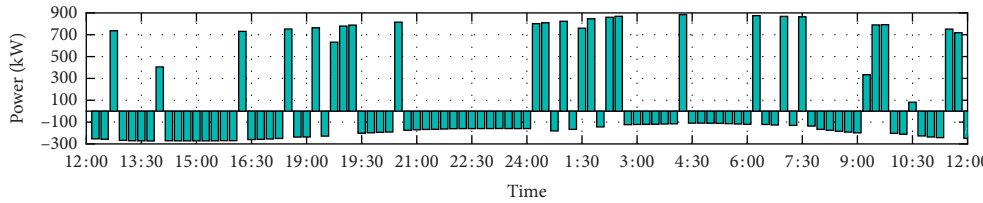

Figure 20: Output power of virtual energy storage with independent participation of air conditioning in Scenario2.

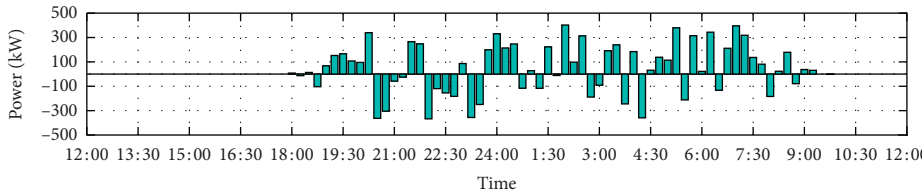

Figure 21: Output power of virtual energy storage with independent participation of electric vehicles in Scenario3.

Table 3: Comparison of the total electricity cost within one day for the constant temperature building in residential area number 1 under four scenarios.

Scenario	Total electricity cost	Electricity saving percentage
Joint virtual energy storage	6532.7	−9.6
Air conditioning virtual energy storage	6672.2	−7.6
Electric vehicles virtual energy storage	6718.7	−7
Without virtual energy storage scheduling	7227.6	—

participation of electric vehicles and air conditioning in virtual energy storage can improve the utilization rate of distributed new energy power generation equipment and improve the economics of electricity consumption.

6. Summary

This paper proposes the use of air conditioning and electric vehicles to jointly participate in virtual energy storage to realize the economic dispatch of energy local area Smart Grid in view of the current status of the controllable load of air conditioning and the load growth of electric vehicles.

Firstly, the virtual energy storage model of thermoelectric conversion with the participation of air conditioning load and the electric energy transfer virtual energy storage model with electric vehicle participation are established. Besides, the rolling optimization idea is introduced to restrict the input and output power of the virtual energy storage with air conditioning and electric vehicle participation.

Secondly, a joint virtual energy storage power optimization model is constructed, and for the solution of the model, in the initialization process of decision variables, due to the condition that dimensional disaster occurred and the initial feasible solution cannot be obtained, a continuous rolling optimization method is proposed for the feasible solution of the high-dimensional complex constraint optimization problem, so that the virtual energy storage power can simultaneously meet the local and global constraints under rolling optimization during the initialization process and thus improve the initialization efficiency.

Finally, the capacity and economy of joint virtual energy storage in residential areas are calculated. The results prove that air conditioning and electric vehicles have the ability to jointly participate in virtual energy storage, and the comparison proves that joint virtual energy storage can effectively improve the economics of electricity consumption. Therefore, the conclusion is that the joint virtual energy storage with the participation of electric vehicles and air conditioning helps improve the economics of consumer electricity consumption.

Data Availability

The data used in this paper comes from the statistics of urban travel data, which has not been published publicly. This paper only takes this data as an example to prove the effectiveness of the proposed method.

Conflicts of Interest

The authors declare that there are no conflicts of interest regarding the publication of this article.

Authors' Contributions

Rui-Cheng Dai and Xiao-di Zhang participated in the algorithm simulation and draft writing. Bi Zhao and Xiao-di Zhang participated in the concept, design, interpretation, and commenting on the manuscript, and the critical revision

of this paper. Jun-Wei Yu, Bo Fan, and Biao Liu participated in the data collection and analysis of the paper.

Acknowledgments

This work was supported by the National Natural Science Foundation of China (Grant nos. 51909199 and 51709215) and the Fundamental Research Funds for the Central Universities (WUT: 2020IVB012).

References

[1] S. Pawan and K. Baseem, "Smart microgrid energy management using a novel artificial shark optimization," *Complexity*, vol. 2017, Article ID 2158926, 22 pages, 2017.

[2] Y. Zou, Y. Chen, and Y. Zou, "Steady-state analysis and output voltage minimization based control strategy for electric springs in the smart grid with multiple renewable energy sources," *Complexity*, vol. 2019, Article ID 5376360, 12 pages, 2019.

[3] L. Xi, Y. Y. Li, and J. L. ChenLu, "A novel automatic generation control method based on the ecological population cooperative control for the islanded smart grid," *Complexity*, vol. 2018, Article ID 2456936, 17 pages, 2018.

[4] J. Lai, X. Lu, X. Yu, and A. Monti, "Stochastic distributed secondary control for ac microgrids via event-triggered communication," *IEEE Transactions on Smart Grid*, vol. 11, no. 4, pp. 2746–2759, 2020.

[5] J. Lai and X. Lu, "Nonlinear mean-square power sharing control for ac microgrids under distributed event detection," *IEEE Transactions on Industrial Informatics*, p. 1, 2020.

[6] D. Choi, A. J. Crawford, V. Viswanathan et al., "Lifecycle comparison and degradation mechanisms of Li-ion battery chemistries under grid and electric vehicle duty cycle combinations," *The Electrochemical Society*, vol. 1, p. 26, 2018.

[7] K. Mai, L. Yin, and Z. Li, "Energy optimization management of grid-connected wind-solar-battery domestic micro-grid based on virtual energy storage," *Distribution & Utilization*, vol. 34, no. 4, pp. 12–18, 2017.

[8] X. Jin, Y. Mu, H. Jia, J. Wu, T. Jiang, and X. Yu, "Dynamic economic dispatch of a hybrid energy microgrid considering building based virtual energy storage system," *Applied Energy*, vol. 194, pp. 386–398, 2017.

[9] X. Zhan, Y. Mu, and H. Jia, "Optimal scheduling method for a combined cooling, heating and power building microgrid considering virtual storage system at demand side," in *Proceedings of the CSEE*, vol. 37, no. 2, pp. 581–590, Barcelona, Spain, April 2017.

[10] X. Ai, Y. Zhao, and S. Zhou, "Study on virtual energy storage features of air conditioning load direct load control," *Proceedings of the CSEE*, vol. 36, no. 6, pp. 1596–1603, 2016.

[11] C. Gao, Q. Li, and Y. Li, "Bi-level optimal dispatch and control strategy for air-conditioning load based on direct load control," *Proceedings of the Chinese Society of Electrical Engineering*, vol. 34, no. 10, pp. 1546–1555, 2014.

[12] O. Erdinç, A. Tascikaraoglu, N. G. Paterakis, Y. Eren, and J. P. S. Catalao, "End-user comfort oriented day-ahead planning for responsive residential HVAC demand aggregation considering weather forecasts," *IEEE Transactions on Smart Grid*, vol. 8, no. 1, pp. 362–372, 2017.

[13] C. H. Wai, M. Beaudin, H. Zareipour, A. Schellenberg, and N. Lu, "Cooling devices in demand response: a comparison of control methods," *IEEE Transactions on Smart Grid*, vol. 6, no. 1, pp. 249–260, 2015.

[14] J. Peppanen, M. J. Reno, and S. Grijalva, "Thermal energy storage for air conditioning as an enabler of residential demand response," in *Proceedings of the 2014 North American Power Symposium (NAPS)*, pp. 1–6, Pullman, WA, USA, September 2014.

[15] J. Lai, X. Lu, X. Yu, and A. Monti, "Cluster-oriented distributed cooperative control for multiple ac microgrids," *IEEE Transactions on Industrial Informatics*, vol. 15, no. 11, pp. 5906–5918, 2019.

[16] J. Lai, X. Lu, X. Yu, and A. Monti, "Stochastic distributed secondary control for ac microgrids via event-triggered communication," *IEEE Transactions on Smart Grid*, vol. 11, no. 4, pp. 2746–2759, 2020.

[17] L. Xin, L. Jingang, and T. Ruoli, "A hybrid constraints handling strategy for multiconstrained multiobjective optimization problem of microgrid economical/environmental dispatch," *Complexity*, vol. 2017, Article ID 6249432, 12 pages, 2017.

[18] G. Xiong, J. Zhang, X. Yuan et al., "A novel method for economic dispatch with across neighborhood search: a case study in a provincial power grid, China," *Complexity*, vol. 2018, Article ID 2591341, 18 pages, 2018.

[19] W.-C. Yeh, M.-F. He, C.-L. Huang et al., "New genetic algorithm for economic dispatch of stand-alone three-modular microgrid in DongAo Island," *Applied Energy*, vol. 263, 2020.

[20] G. Ruan, H. Zhong, J. Wang, Q. Xia, and C. Kang, "Neural-network-based Lagrange multiplier selection for distributed demand response in smart grid," *Applied Energy*, vol. 264, Article ID 114636, 2020.

[21] F. Pallonetto, M. De Rosa, F. Milano, and D. P. Finn, "Demand response algorithms for smart-grid ready residential buildings using machine learning models," *Applied Energy*, vol. 239, pp. 1265–1282, 2019.

[22] W. Zhang, J. Lian, C.-Y. Chang, and K. Kalsi, "Aggregated modeling and control of air conditioning loads for demand response," *IEEE Transactions on Power Systems*, vol. 28, no. 4, pp. 4655–4664, 2013.

[23] N. Ruiz, I. Cobelo, and J. Oyarzabal, "A direct load control model for virtual power plant management," *IEEE Transactions on Power Systems*, vol. 24, no. 2, pp. 959–966, 2009.

[24] J. Lai, H. Zhou, and W. Hu, "Synchronization of hybrid microgrids with communication latency," *Mathematical Problems in Engineering*, vol. 2015, Article ID 586260, 10 pages, 2015.